Semiconductors, Vol. 35, No. 9, 2001, pp. 1095–1105. Translated from Fizika i Tekhnika Poluprovodnikov, Vol. 35, No. 9, 2001, pp. 1143–1153.

LOW-DIMENSIONAL SYSTEMS

Type-II Ge/Si Quantum Dots

A. V. Dvurechenskiæ* and A. I. Yakimov

Institute of Semiconductor Physics, Siberian Division, Russian Academy of Sciences, Novosibirsk, 630090 Russia

** e-mail: dvurech@isp.nsc.ru*

Submitted February 14, 2001; accepted for publication February 15, 2001

Abstract—The electronic structure of spatially indirect excitons, multiparticle excitonic complexes, and negative photoconductivity in arrays of Ge/Si type-II quantum dots (QDs) are considered. A comparison is made with the well-known results for type-II III–V and II–VI QD heterostructures. The following fundamental physical phenomena are observed in the structures under study: an increase in the exciton binding energy in QDs as compared with that for free excitons in homogeneous bulk materials, a blue shift in the excitonic transitions during the generation of multiparticle complexes (charged excitons, biexcitons), and the capture of equilibrium carriers to localized states induced by the electric field of charged QDs. © *2001 MAIK "Nauka/Interperiodica"*.

1. INTRODUCTION

The relative position of energy bands on both sides of a heterointerface in a heterosystem is determined by the structure and composition of the constituent semiconductor materials [1]. If the lowest energy states of electrons and holes in the band diagram are located in one of the two materials forming the system, the system is referred to as a type-I heterostructure. If the lowest energy state for electrons is associated with one material and that for holes, with the other, the system is of type II. Therefore, in type-II heterostructures with two heterojunctions, a potential well can be formed only for one type of carrier, electron or hole with a barrier existing for the other type of carrier. In the literature, the band diagram of such a structure is often staggered, implying similar energy steps in conduction or valence band discontinuities: ascending or descending energy steps at the heterointerface for each of the bands.

In clusters of a material introduced into the bulk of another material, the carrier motion is confined in all the three directions. If the cluster size is comparable with the de Broglie wavelength of an electron, hole, or with the Bohr radius of an exciton, then the inclusions are referred to as quantum dots (QDs) [2] and semiconductor structures with such clusters are called QD heterostructures [1]. In contrast to quantum-well (QW) and quantum-wire heterostructures (two-dimensional and one-dimensional systems), the properties of electrons and holes in QD heterostructures cannot be described as a gas of quasiparticles. A fruitful concept in this case is that of localized states. The electron or hole localization radius in a nanocluster is comparable with the cluster size, and frequently it exceeds the Bohr radius of single impurity atoms with shallow levels in homogeneous bulk semiconductors. On the other hand, the energy level in a QD may be deep, and this is one more feature of QDs as deep-level impurity centers. Owing to specific features mentioned above, the study of QD heterostructures now constitutes a separate branch of condensed-matter physics.

Charge localization in a QD modifies the potentials in the neighboring space. This gives rise to a potential well for carriers of opposite sign around a QD and leads to the formation of bound states in this well. In type-II heterostructures, localized states for holes and electrons emerge in self-consistent potential wells on different sides of the heterointerface. Electrons and holes in these states are spatially separated, and the transition between these states is spatially indirect.

Finding the energy spectrum parameters, analyzing the kinetics of transitions between electron states and the interaction of elementary excitations, and revealing the correlation effects constitute the main part of the contemporary fundamental studies of QDs. The utmost attention is attracted by $In_xGa_{1-x}As/Al_yGa_{1-y}As$ systems owing to the prospects for their application in semiconductor lasers (see, e.g., reviews [1, 3] and references therein). Type-II QDs formed in (In,Ga,Al)Sb/GaAs, (Al,In,As)/InP, (Ga,In,As,Sb)/GaSb, Ge/Si, and ZnTe/ZnSe heterostructures are less understood [4–11]. Heterostructures with compound semiconductor QDs are of particular importance for optoelectronics. Ge/Si heterosystems with QDs open up new prospects for micro- and nanoelectronics [12–15].

The electronic processes in QD systems have mainly been studied by optical methods [1, 3, 5, 6]. Our investigations were the first to apply electrical methods to reveal the discrete energy spectrum in an array of self-organized QDs and the Coulomb interaction in charge transport and to determine the carrier capture cross sections of localized states [4, 13, 15, 16]. The existence of a wealth of data concerning the surface and

1063-7826/01/3509-1095$21.00

the phase boundaries for Ge and Si [17], as well as the possible application of the developed techniques in modern silicon technology of discrete devices and circuits, makes investigating the Ge/Si system a priority. In this communication, we present data obtained in studying electronic processes, mainly in the Ge/Si system, by means of a set of optical and electrical techniques. The results are compared with the available data for other QD systems.

2. OBJECTS AND METHODS OF STUDY

Presently, the most promising method to produce an array of QDs is based on the self-organization of semiconductor nanostructures in heteroepitaxial systems [1, 5, 14]. Elastic strains in an epitaxial film and islands on its surface are crucial both for a morphological transition from a flat film to island growth (Stranski–Krastanow mode) and for further changes in the size, shape, and spatial distribution of the islands. An important stage in the sequence of the occurring kinetic transitions is the formation of coherent (defect-free) three-dimensional (3D) islands with a uniform size, which gives nanometer islands with quantum confinement energy of about 100 meV [13, 15]. This value noticeably exceeds the room-temperature thermal energy of particles (26 meV); therefore, the thermal redistribution of carriers over localized states within an energy window on the order of k_0T (k_0 is the Boltzmann constant, T the temperature) can be disregarded. These systems enable room-temperature operation of QD structures exhibiting temperature-insensitive device characteristics over a wide temperature range [18].

We have found the conditions of Ge heteroepitaxy onto (110) Si that provide a 3×10^{11} cm^{-2} sheet concentration of clusters [14]. The size distribution of germanium islands was studied by STM. The average size of islands (pyramid base) was 15 nm, and the pyramid height was 1.5 nm, with deviations being no more than 17%. Typical conditions of Ge/Si structure formation included homoepitaxy at 800°C onto (100) Si at a rate of 1–2 monolayers per second (ML/s); Ge heteroepitaxy at 300°C, 0.2 ML/s; and Si epitaxy over the Ge islands at 500°C. The effective thickness of the Ge layer was varied within d_{eff} = 0–20 ML. In Ge/Si QD heterostructures, holes are localized in Ge nanoclusters. Nonuniform structural strains (resulting from a 4% lattice mismatch between Ge and Si) and the positive charge created in Ge by holes can induce a potential well for electrons in the conduction band of silicon in the vicinity of the heterojunction.

3. SPATIAL DISTRIBUTION OF ELASTIC STRAINS

Nonuniform elastic strains in heterostructures can cause significant changes in the electrical and optical properties as a result of the energy-spectrum modification by about 0.1 eV [19, 20]. Furthermore, nonuniform strains favor the spatial ordering of nanoclusters during the formation of multilayer structures [21]. Therefore, determining the fields of elastic strains is a necessary step in both calculating the band structure of self-arranged QDs and modeling the epitaxy on strained surfaces. The elastic strain fields in Ge nanoclusters and in their environment were calculated by means of an original method relying upon Green's tensor of the elastic problem [22]. The sizes of the QDs studied are so small that the continuum approximation is inapplicable to description of the elastic properties of the system. The strain was calculated using the Keating [23] potential, taking into account the atomic structure of the substance. To reduce the calculation error introduced by the finite crystal volume, we sought the deformational field as a convolution of some auxiliary function with the Green's function (Green's tensor) of the elastic atomistic problem. This method yields the distribution of strain at the atomic level for a system containing inclusions of one material in the matrix of another. The crystal anisotropy and the different elastic properties of the medium with inclusions of another phase are taken into account.

The problem was solved for the objects studied in our experiments: germanium QDs had the form of tetrahedral pyramids with an 11° slope on their lateral faces, a base size of 15 nm (in the growth plane), and a height of 1.5 nm. A QD sheet located on top of a 0.7-nm-thick wetting Ge layer was embedded in bulk crystalline silicon. The solution was obtained for a single QD, which means that the superposition of elastic strain fields from the array of surrounding QDs was disregarded.

It was established that the strain inside a Ge nanocluster is tensile in the direction of structure growth (z direction) and compressive in the lateral direction (xy plane) (Fig. 1). The highest strain exists along the outline of the pyramid base in the growth plane, and the most relaxed is in the vicinity of the apex. The highest strain in the silicon environment of a QD is located in the vicinity of the pyramid apex. Calculations show that the strain in the central part of the pyramid is practically independent of the Ge nanocluster size for the pyramid base within 6–15 nm. Near the edge of the pyramid base, the strain grows as a logarithm of the base size.

Recently, results obtained in calculating the strain in the Ge/Si QD system with the use of two empirical potentials—Keating and Stillinger–Weber—have been compared [24]. Both methods yield similar results for the lateral tensor components, with a quantitative difference found for the normal tensor components. As a result, the authors of [24] recommended that the Stillinger–Weber potential should be used for Ge nanoclusters with a pyramid base smaller than 10 nm.

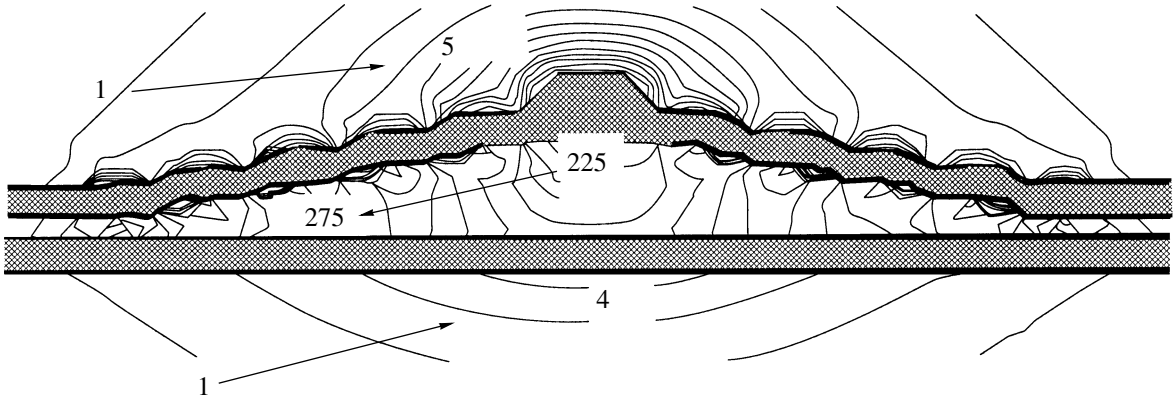

Fig. 1. Distribution of elastic energy in a QD and its neighborhood in the (100) plane passing through the pyramid axis. The figures indicate the energies per atom in units of 10^{-4} eV. Arrows show the directions of increasing energy [22].

4. ELECTRONIC STRUCTURE OF SPATIALLY INDIRECT EXCITON

For homogeneous bulk semiconductors, the term "indirect exciton" is applied to an excited electron state formed upon indirect optical transitions [25]. In type-II QDs, there exist optical transitions that are indirect in the real space. The same transitions may either be indirect in the *k*-space, where *k* are the wave vector components (e.g., in Ge/Si and GaAs/AlAs (the latter system is of type II for QD size less than 56 Å and type I for QDs larger 56 Å [8]) or direct (e.g., in the InAs/GaSb system with InAs QDs, belonging to type II at QD size less than 87 Å [8], and in GaSb/GaAs [6]). The excited states formed upon optical transitions, with electron and hole localized on different sides of the heterointerface, are called spatially indirect excitons.

To obtain the absorption spectrum of a nanocluster containing N electron–hole pairs, it is necessary to solve the Schrödinger equation with a Hamiltonian that includes the kinetic and potential energy of noninteracting electron and hole and the energy of their interaction [26].

Wavefunctions and the energy spectrum of electrons and holes in spatially indirect excitons were simulated numerically for a Ge pyramid in Si, with dimensions specified in Section 3. The band offsets at the Ge/Si heterojunction were calculated on the basis of the obtained spatial distribution of elastic strains both inside and outside the pyramidal QD as well as on the known strain potentials for Si and Ge [27]. The elastic strains in Si lift the 6-fold degeneracy of the Δ valleys, with 4- and 2-fold-degenerate valleys were formed. The 2-fold degenerate valleys are oriented along the [001] and $[00\bar{1}]$ directions and lie lower in energy than states in the conduction band of Ge (the minimum of the conduction band). The maximum of the valence band is formed by heavy holes from Ge nanoclusters.

The states of spatially indirect excitons and excitonic complexes are described in terms of the effective mass method. A system of 3D Schrödinger equations was solved: two equations for a single exciton, three equations for an exciton–hole complex, and four equations for two excitons in a QD.

The interaction between charged particles was simulated by a static screened Coulomb potential. The conduction band offset between the corresponding Δ minima of unstrained Ge and Si was 340 meV, and the valence band offset was 610 meV. The electron effective masses in the Si conduction band were $m_{xy} = 0.19m_0$ in the QD growth plane, and $m_z = 0.92m_0$; the hole effective masses in the valence band were $m_{xy} = 0.39m_0$ and $m_z = 0.2m_0$. Only heavy holes were considered, because the light-hole states were close to the valence band edge of Si. The exciton wavefunctions were taken in the Hartree approximation as a product of the electron and hole wavefunctions.

For the case of a single exciton, the calculations demonstrated that the electron is localized in a QD in the region of the maximal strain in Si (in the vicinity of the Ge pyramid apex), and the hole is confined near the pyramid base. In a two-exciton complex, the repulsion of electrons causes their spatial separation; therefore, the second electron is bound near the interface between Si and the continuous Ge layer, on which the pyramids lie (Fig. 2). In this region, there exists a second local minimum of the conduction band induced by elastic strains originating from the lattice mismatch between Ge and Si. In the vicinity of the pyramid apex, this local extremum is shallower than the first one.

The calculations also demonstrated that the electron binding energy in exciton formation $E_t = 38$ meV. The main contribution to the electron localization energy near the Ge/Si heterointerface comes from the electron–hole Coulomb interaction (the exciton binding energy is 29 meV). The remaining part (9 meV) is due

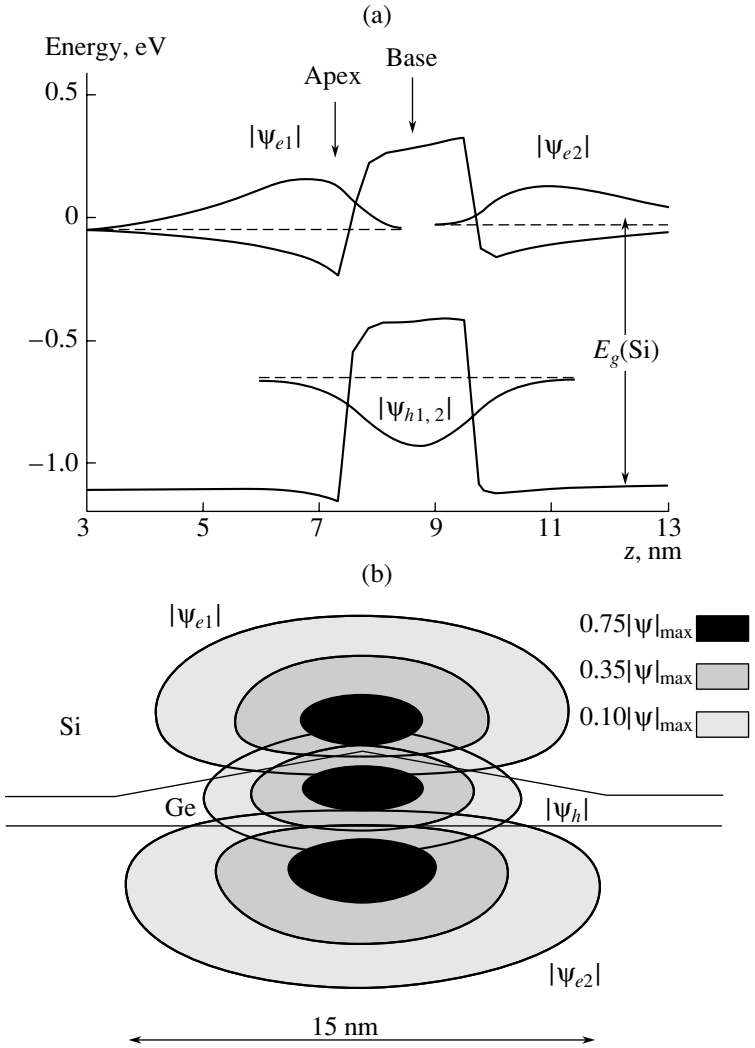

Fig. 2. (a) Calculated potential profile (along the *z*-axis passing through the apex of a Ge pyramid) in which electrons and holes move, constituting an excitonic complex. (b) 2D image of the modulus of electron and hole wavefunctions ($|\psi_e|$ and $|\psi_h|$) in the cross section of a QD and its neighborhood. The extents of black denote regions at whose boundaries the wavefunctions decay to 75, 35, and 10% of the maximum value $|\psi|_{max}$ [26, 28].

to the contribution from the nonuniform distribution of strains to the potential well formation at the Ge/Si interface. In fact, the latter value is the energy of the electron state in the potential well of a neutral Ge nanocluster.

5. EXCITONIC ABSORPTION

The absorption peak related to the electron transition from the Ge QD valence band to the Si conduction band with the formation of an exciton is observed at 760–770 meV [26, 28]. This transition yields the ground state of a spatially indirect exciton (a hole is formed in the *H*0 ground state in a Ge nanocluster, and an electron passes into the *E*0 ground state in Si at the heterojunction). A weaker absorption peak in the range 850–860 meV is attributed to an excited exciton, with an electron and a hole in both the *H*1 and *E*1 excited states. The band width of 50–70 meV is presumably due to fluctuations of the shape and size of Ge clusters.

5.1. Single Exciton

The oscillator strength *f* of the excitonic transition in Ge/Si was determined from the optical absorption data. The obtained value of 0.5 is about 20 times less than the oscillator strength for direct (in real and *k*-space) excitons in InAs/GaAs QD structures having $f = 10.9$ [29, 30]. The oscillator strength of an excitonic transition is proportional to the squared overlap integral of the electron and hole wavefunctions. In InAs/GaAs QD structures, the electron and hole are localized within the same nanocluster. Therefore, the overlap of their wavefunctions is relatively large, about 80% [31]. The solution of a self-consistent problem for Ge/Si system

yields a 15% overlap of the electron and hole wavefunctions [28]. The smaller overlap in Ge/Si (compared with that in InAs/GaAs) is a direct consequence of the spatial separation of the electron and hole in type-II heterostructures. At the same time, the overlap in type-II QD structures depends on the height of the barrier separating the electron and the hole as well as on the QD size. Evidently, an infinite barrier corresponds to complete separation of wavefunctions and zero overlap. This situation virtually does not occur in the discussed structures with finite barrier height.

Of more interest is the dependence of the overlap factor on the QD size at constant (finite) barrier. The wavefunction is "squeezed out" of the QD volume with a decreasing QD size or barrier height. This enhances the overlap of the electron and hole wavefunctions and makes the correlation of their motion stronger. According to calculations made in [9], the overlap factor starts to grow dramatically when the ratio of the QD size to the Bohr radius of the hole becomes less than four. The overlap factor decreases with an increasing QD size (in Bohr radius units). The conclusion that the oscillator strength may become appreciable in type-II QDs was also made on analyzing the kinetics of the photoluminescence decay in an array of pyramidal GaSb/GaAs QDs [7].

The measured absorption probability ($\alpha = 1.6 \times 10^{-4}$) allows the evaluation of the effective interband absorption cross section in Ge QDs to be $\sigma_{ph} = \alpha/2\sigma_{qd} = 2.5 \times 10^{-16}$ cm^2, where σ_{qd} is the density of QDs. This value exceeds the typical photoionization cross sections of deep levels in Si (~10^{-17} cm^2 [32]) by more than an order of magnitude. This fact is an indication that the absorption band at 750–850 meV is not associated with defects or impurities in Si. Another argument in favor of the developed concept is furnished by experiments on annealing of Ge/Si QD structures. The absorption band at 750–850 meV is not affected by a 30-min annealing at 500°C, whereas many point defects in Si are annealed at this temperature, being transformed into more intricate complexes.

5.2. Multiparticle Excitonic Complexes

The existing methods for studying QD structures make it possible to create conditions under which several charged excitons are formed in a single QD. For example, holes are accumulated at the top of the valence band in Ge nanoclusters in injection of holes into Ge/Si QD structures [28]. An 11-meV blue shift of the line of main excitonic absorption (*H*0–*E*0) was observed in single-charged Ge QDs. Figure 3 shows the shift of the excitonic absorption peak in relation to the average number of holes per QD. The transition energy increases sharply when an extra hole appears in the QD ground state, thus enabling the formation of a charged (⟨2 holes⟩–electron) excitonic complex on photon absorption. The observed blue shift is accounted for by the dependence of the excitonic transition energy on the QD charge state: generation of an exciton in a hole-containing QD requires more energy than that in a neutral QD. The positive sign of this effect is a specific feature of type-II QDs, which means that the energy of the hole–hole Coulomb interaction in a QD—E_{hh} (repulsion)—exceeds the hole–electron interaction energy E_{eh} (exciton binding energy).

This result contradicts the previous data for spatially direct excitons in InAs/GaAs QD arrays, when the energy of the excitonic transition decreases upon the formation of excitonic complexes [29, 30]. In the case of direct excitons, the electron–hole interaction dominates and the absorption line of a charged exciton is redshifted [29]. For type-II QDs, it would be natural to expect that $E_{hh} > E_{eh}$, owing to the spatial separation of an electron and a hole. This will cause a shift of the excitonic line to shorter wavelengths upon the formation of a charged complex.

The additional energy of the charged exciton as compared with a neutral one is determined by the difference $E_{ex\text{-}h} = E_{hh} - E_{eh}$, equal to the experimentally found 11-meV shift of the optical transition. Taking into account that $E_{hh} = 36$ meV [33], we obtain the electron–hole interaction energy $E_{eh} = 25$ meV, which correlates with the solution of the self-consistent problem. The obtained E_{eh} exceeds the free exciton binding energy for Ge by nearly an order of magnitude and is twice that for Si.

The optical absorption peak of the excited exciton state is shifted to shorter wavelength to a lesser extent upon the appearance of a hole in the QD ground state (Fig. 3). This is due to a weaker electron–hole interaction because of the smaller overlap of their wavefunctions in states with large localization radii.

An alternative way to produce excitonic complexes in a single QD consists in the additional illumination of a structure with interband light when measuring the absorption spectra [28]. Additional illumination leads to filling of hole levels in a Ge QD and the electron levels in Si in the vicinity of the heterojunction with nonequilibrium carriers. Thus, optical absorption of radiation causing *H*0–*E*0 excitonic transition in a structure containing a single exciton gives rise to a biexciton, whereas injection of holes in optical absorption yields an exciton–hole complex.

A stronger blue shift of the excitonic absorption line was observed under the additional illumination as compared with that in the case of injection of holes into a QD. If we assume that, during the formation of an exciton–exciton complex, a pair of holes is in the ground state of the Ge QD and a pair of electrons is in one QW at the phase boundary, then the energy of exciton–exciton interaction increases by

$$\Delta E_{ex\text{-}ex} = E_{hh} + E_{ee} - 2E_{eh},$$

where E_{ee} is the energy of electron–electron interaction in the QD. Using the experimental values $\Delta E_{ex\text{-}ex}$ =

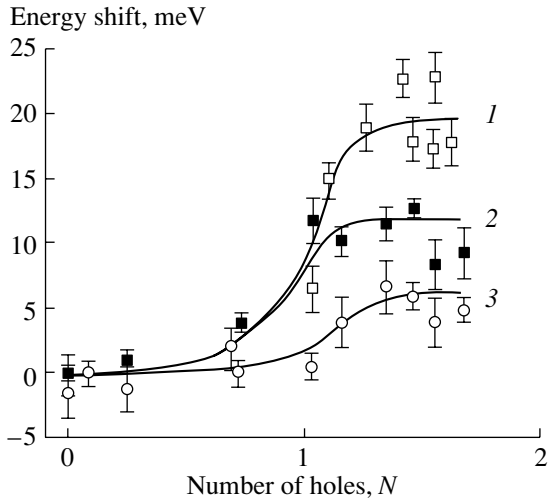

Fig. 3. Shift of excitonic absorption peak vs. the average number of holes per QD in a Ge/Si structure (1) under illumination and with injection of holes for (2) the ground state and (3) excited state of exciton.

20 meV (blue shift of the excitonic absorption line under additional illumination), E_{hh} = 36 meV, and E_{eh} = 25 meV, we obtain E_{ee} = 34 meV, i.e., $E_{ee} \approx E_{hh}$.

However, this result contradicts rather obvious concepts. The localization radius of a hole (localized within a Ge nanocluster) must be considerably smaller than the radius of the electron localization at a QD. Since the interaction energy is inversely proportional to the characteristic radius of the wavefunction, the relation $E_{ee} < E_{hh}$ must be always valid. The estimated value E_{ee} = 34 meV indicates that the above assumption where two electrons are present in the same QW is wrong. If the second electron is in another potential well at the heterointerface, additional single-particle energies E_1, E_2 for each electron in its own potential well must appear in the relation for $\Delta E_{\text{ex-ex}}$, and the corresponding potential wells are not equivalent (see Sec. 4). In this case, the expression for $\Delta E_{\text{ex-ex}}$ must include one more positive term $(E_2 - E_1)$ and the E_{ee} value obtained using this relation may be substantially smaller than E_{hh}. As shown by calculations of the electronic configuration of the exciton (Sec. 4), the first of the two electrons is localized in Si at the apex of the Ge pyramid; the second, under the pyramid base.

The calculated interaction energy of two electrons E_{ee} = 19 meV. Then, using the known interaction energies E_{hh} = 36 meV and E_{eh} = 25 meV, we obtain $\Delta E_{\text{ex-ex}}$ = 5 meV. This means that, if the electrons had equal single-particle energies, the excitonic absorption line would shift by only 5 meV upon the formation of an exciton–exciton complex. The experimental value of this shift is 20 meV. Therefore, the "blue" shift observed upon formation of two excitons in a single QD is related to the higher quantum-confinement energy of the second electron as compared to that of the first, with the difference in energies arising from the localization of two electrons in nonequivalent potential wells.

6. NEGATIVE PHOTOCONDUCTIVITY

Along with the spatial separation of the exciton ground state in Ge/Si QDs, solving the self-consistent problem to determine the electron and hole energy spectrum yielded results that allowed us to predict and experimentally find the effect of negative interband photoconductivity [34, 35] consisting in that the conductivity of the QD layer decreased under additional illumination. For most data on the photoconductivity in semiconductors, the conductivity of a material increases under interband illumination. It was found that a QD containing N holes can trap $N + 1$ electrons, with the energy of the extra electron dependent on the number of holes. Figure 4 shows the calculated binding energy of the $(N + 1)$-th electron in the vicinity of a Ge island containing N holes in relation to the number of holes in a QD. Since interband illumination generates electrons and holes in pairs (i.e., at equal concentrations), such an additional (and, consequently, unfilled) state would be a trap for the equilibrium conduction-band electrons.

Let us consider n-Si with undoped Ge nanoclusters introduced into it (Fig. 5). The dark conductivity of the system is determined by free electrons excited into the Si conduction band via thermal ionization of donors. As mentioned above, even in the absence of holes in the QDs, a shallow electron level with the binding energy $E_t \approx 9$ meV exists at the Si/Ge heterointerface owing to nonuniform strains that create a potential well for electrons (Fig. 4). Therefore, the equilibrium concentration of electrons in the conduction band is lowered because of the electron capture to this level. In the absorption of light, which induces interband transitions to form electron–hole pairs, holes are accumulated in Ge QDs, charging them positively. Consequently, the potential wells for electrons appear in Si at the Ge/Si heterointerfaces, with photoelectrons accumulated in these wells (Fig. 5b). With an increasing number of holes in the islands (on raising the illumination intensity), the energy depth of the "excess" electron level increases (at $N < 3$) (Fig. 4). Since the electron filling of the level increases as its energy becomes lower, the electron concentration in the conduction band must decrease with the conductivity of the system.

Negative photoconductivity in semiconductors was first observed by A.F. Ioffe and A.V. Ioffe, who demonstrated that, under conditions of strong surface absorption of light, a situation is possible when a majority of the carriers recombine in the skin layer and the inward diffusion of minority carriers enhances the recombination in the bulk, i.e., suppresses the bulk conductivity [36]. Since, in our case, the recombination time in the

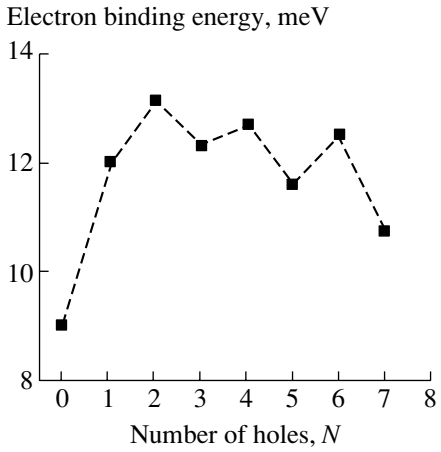

Fig. 4. Binding energy of the (N + 1)-th (excess) electron at the Ge/Si interface vs. the number of holes in Ge nanocluster, N [28].

surface layer with QDs is longer than that in the bulk [35], this mechanism is inoperative.

Another known mechanism of the negative photoconductivity observed earlier in bulk p-Ge samples is the modulation of the mobility of hot holes upon carrier excitation of carriers from a heavy- to a light-hole band [37, 38]. However, this situation only occurs under intraband illumination (photon energy ≈120 meV).

Negative photoconductivity associated with recharging of scattering centers by light was also observed in layered GaSe and InSe crystals [39].

It should also be noted that a decrease in the carrier concentration in 2D subbands and an increase in the structure resistance under illumination with $h\nu > E_g$ photons has been observed in 2D systems based on $In_{0.25}Ga_{0.75}Sb/InAs$ [40], $InAs/Al_{0.5}Ga_{0.5}Sb$ [41], and $ZnS_{1-x}Se_x/Zn_{1-y}Cd_ySe$ heterostructures [42]. The effect was ascribed to the capture of photoexcited electrons from the quantum valley to electronic traps within the barrier. The presence of electronic traps accounted for the negative photoconductivity in PbTe [43] and $Pb_{1-x}Sn_xTe\langle In\rangle$ films [44].

The nature of a trapping center is specific to each particular material. For example, the traps in GaAs structures are, presumably, DX-centers [45]. We were the first to demonstrate [34] that it is possible for photoinduced traps in type-II QD arrays of one type of carriers to be unrelated to structural defects but to arise from fundamental quantum effects.

To verify the proposed concepts, we studied the photoconductivity of epitaxial Ge/Si structures grown on (001) Si substrate with phosphorus concentration $N_s \approx 10^{15}$ cm^{-3}. The substrate thickness was L_s = 300 μm. The structures comprised ten layers of Ge islands interspersed with 30-nm-thick Si layers. The overall thickness of the epitaxial layer was $L_{epi} \approx$ 0.3 μm. The donor (Sb) concentration in the epitaxial Si was $N_{epi} \approx 2.5 \times 10^{16}$ and 8×10^{16} cm^{-3}. The sheet nanocluster density was $\sigma_{qd} = 3 \times 10^{11}$ cm^{-2}.

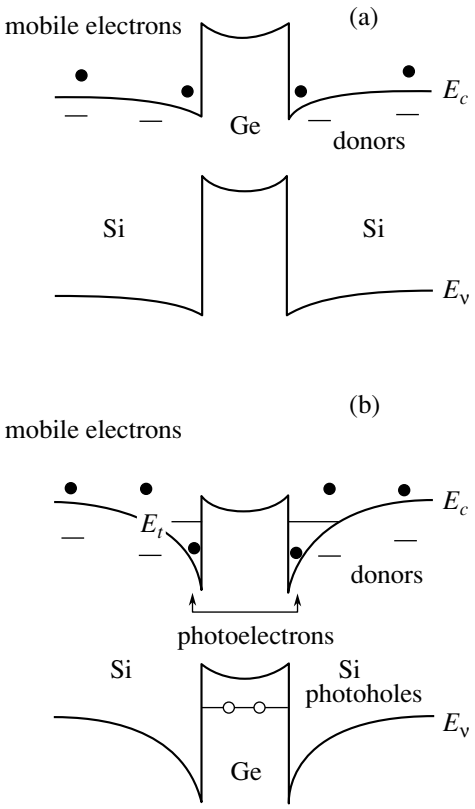

Fig. 5. Band diagram of Ge/n-Si heterostructure with Ge QDs (a) in the dark and (b) under illumination. Solid circles, electrons; open circles, holes.

A GaAs LED with peak emission at ~0.9 μm was used as a light source. The LED emission intensity was modulated at a frequency of 2 kHz. The lateral photoconductivity was recorded at the modulation frequency in the linear (Ohmic) region of the current–voltage characteristic (at electric field strengths no more than 0.5 V/cm). Electric contacts were fabricated by Al sputtering, with subsequent heating of the structure to 450°C in an N_2 atmosphere. To preclude the illumination of contacts, which could induce spurious negative photoconductivity [46], the contacts and the adjacent region were screened with an opaque coating.

Figure 6 presents the relative photoconductivity $\Delta G/G$ as a function of the illumination intensity (P) for Ge/n-Si QD structures at different temperatures (solid and dotted lines) and for a sample having no epitaxial layer with QD-islands at 77 K (dashed line). In this sample, the photoconductivity is positive and increases practically linearly with P. A negative photoconductivity is observed in the structures with Ge nanoclusters at illumination intensities $P < 100$ mW/cm^2.

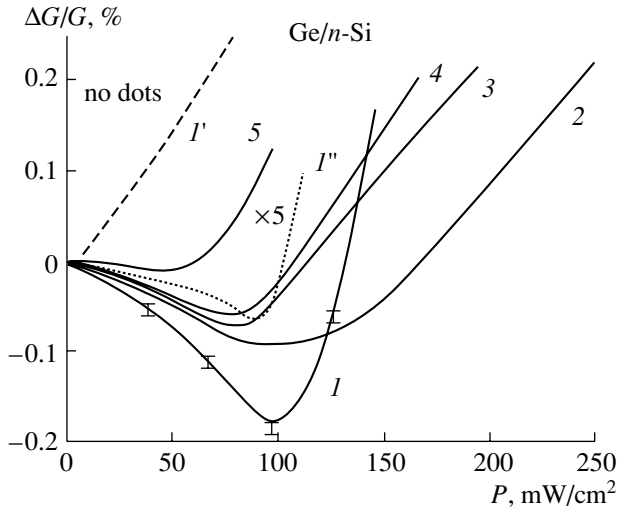

Fig. 6. Relative photoconductivity vs. the interband illumination intensity in *n*-Si with QDs, at temperatures *T*: (*1*, *1*', *1*") 77, (*2*) 87, (*3*) 99, (*4*) 102, and (*5*) 180 K. Antimony concentration: (*1*–*5*) 2.5×10^{16} and (*1*") 8×10^{16} cm^{-3}. (*1*') Structure without QDs.

The negative photoconductivity is not observed in *p*-layers with Ge QDs. Figure 7 shows the photoconductivity of a Ge/*p*-Si structure as a function of the illumination intensity. The conditions of sample growth were similar to those for the Ge/*n*-Si structures, with the exception of the conduction type of the substrate and the top epitaxial Si layer with Ge islands (boron acceptor concentration ~10^{15} cm^{-3}). As seen, there is no region of negative photoconductivity in these curves. Instead, an extended region with a small positive photoconductivity is observed, after which there occurs a sharp rise in the photocurrent. Such a behavior at a small illumination intensities is associated with the capture of both types of nonequilibrium carriers to bound states in the vicinity of Ge islands (holes tied to states inside the islands; electrons tied to states at the Ge/Si heterointerface). The rise in photoconductivity at high illumination intensities is due to the filling of electronic levels and the generation of free nonequilibrium electrons. This result also indicates that the observed negative photoconductivity is not related to the carrier mobility modulation under illumination.

The described mechanism of negative photoconductivity is only operative in type-II QDs, since both electrons and holes are localized in one semiconductor in type-I heterostructures irrespective of the charge state of QDs.

7. COMPARISON OF PARAMETERS OF PHOTOSENSITIVE QD STRUCTURES

It is of interest to compare the available data on the photon absorption cross sections and detectivity for structures with both types of QDs. For the Ge/Si system, the wavelength range 6–20 μm corresponds to interlevel transitions [47, 48], and the range 1.7–3 μm, to indirect (in real and *k*-space) interband transitions. As seen, the larger cross section corresponds to transitions between states related to the vertical confinement of particle motion (in the *z*-direction). The exceptions are InAs/InAlAs and Ge/Si systems, in which large cross sections of photon absorption have also been observed in laterally polarized transitions (light beam polarization in the *xy*-plane of the QD sheets). This property allows us to regard these systems as good can-

Parameters of photosensitive structures with QDs and superlattices

QD systems (QD/matrix)	*T*, K	λ_m, μm	*n*	σ_{ph}, 10^{-15} cm^2	*D**, 10^8 cm Hz$^{1/2}$/W	Source
InAs/GaAs	300	6	*z*	3		[51]
InAs/GaAs	90	7	*z*	3		[52]
InAs/GaAs	120	11	*xy*	0.16		[53]
InAs/GaAs	120	6–8	*xy*	0.25		[53]
InAs/InAlAs	300	13.8	*xy*	15		[54]
InAs/GaAs	300	10.6	*xy*		0.3	[55]
InGaAs/InGaP	77	5.5	*xy*		0.47	[56]
Ge/Si	77	6	*xy*	200		[50]
Ge/Si	300	10–20	*xy*	0.8	0.7–1.7	[57]
Ge/Si	300	1.7–3	*xy*	1		[57]
2D systems						
$Si_{1-x}Ge_x$/Si	77	9	*z*		10	[58]
InAs/GaSb	77	10.3	*z*		13	[59]

Note: *T* is the temperature of the experiment, λ_m is the wavelength in the spectral sensitivity peak, *n* is the radiation polarization, σ_{ph} is the cross section of photonic absorption, *D** is the detectivity.

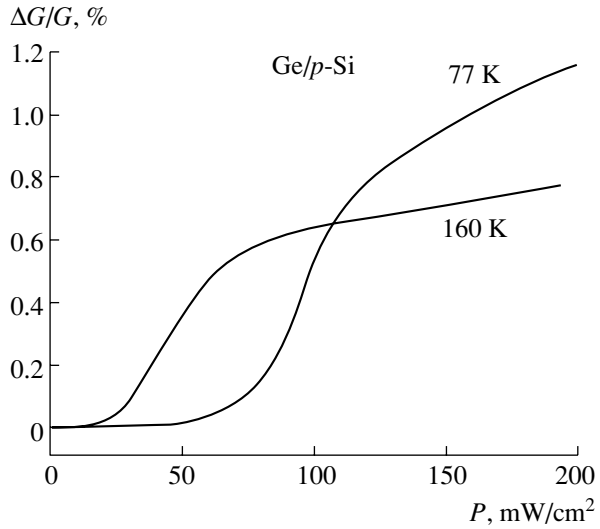

Fig. 7. Relative photoconductivity vs. the interband illumination intensity for a Ge/*p*-Si structure with Ge QDs.

didates for the fabrication of photodetectors ensuring the absorption of radiation under normal incidence of light onto a structure [49, 50] (see table). A similar conclusion for the Ge/Si heterostructures follows from a comparative analysis of the detectivities D^* of photodetectors with different kinds of QDs, presented in the table. It is seen that the room-temperature D^* for Ge/Si system is more than twice as large as the value obtained for InAs/GaAs QDs (type-I heterosystem).

A comparison of the detectivities of photodetectors based on structures with 2D electron gas and QD structures (see table) shows that the D^* for 2D systems is about an order of magnitude higher than the values that have been achieved in QD structures. We believe that this is due to the higher carrier concentration in 2D superlattices ($\sim 10^{12}$ cm^{-2}). The photosensitive structures in this work contain no more than 10 QD layers. Simple evaluations show that raising the number of Ge QD layers must bridge the detectivity gap.

8. CONCLUSION

The performed investigations of type-II QD systems have been aimed at determining the electronic spectra of excitations and their interactions and finding the physical parameters characterizing the class of zero-dimensional structures under study. The fundamental physical phenomena specific to type-II QDs are as follows:

(1) a higher exciton binding energy as compared with the free exciton binding energy in homogeneous bulk semiconductors, which results from the confinement of an electron and a hole, and a higher contribution of the overlap of their wavefunctions, resulting from their mutual penetration into a potential barrier of finite height;

(2) a blue shift of the excitonic transition in the formation of exciton–hole and exciton–exciton complexes; spatial separation of electrons in a biexciton in the Ge/Si structure;

(3) negative photoconductivity under interband illumination due to the capture of equilibrium carriers to localized states formed by the field of charged QDs.

Further, there exist a number of phenomena that have been discovered in type-II QDs but which may also be characteristic of type-I QDs:

(1) a larger cross section of photon absorption as compared with that associated with point defects in bulk semiconductors;

(2) a blue shift of the interlevel absorption line in QDs at a higher carrier concentration (lateral depolarization effect) [26, 47, 48, 57];

(3) a larger cross section of carrier trapping into QDs [60];

(4) an oscillatory behavior of conductivity in an array of tunnel-coupled QDs when varying the extent their filling [61, 62];

(5) a universal character of the preexponential factor in the temperature dependence of conductivity along the tunnel-coupled QD sheets equal to e^2/h [63].

We should also mention the most important (as regards application in semiconductor devices) results the studies performed:

(1) a "single-electron" FET with a channel of tunnel-coupled QDs [61, 62];

(2) absorption of light in its normal incidence onto a QD structure [49];

(3) IR photodetectors operating on optical transitions between the quantum confinement levels and on interband transitions; control by means of external bias over the spectral range of light absorption [49].

Important technological features associated with the development of this line of research consist of self-organization in low-temperature epitaxy, the investigations of controlling the nanocluster formation by means of irradiation with low-energy ions during molecular-beam heteroepitaxy [64], and application of silicon-on-insulator structures.

ACKNOWLEDGMENTS

The elastic strain fields were calculated, and the self-consistent problem of the energy spectrum was solved by A.V. Nenashev.

This study was supported by the Russian–Ukrainian Scientific and Technological Program "Nanophysics and Nanophotonics" (project no. 2000-F2), Program "Physics of Solid-State Structures" (project no. 98-1100), Program "Universities of Russia—Basic Research" (project no. 015.01.01.34), and the Russian Foundation for Basic Research (project no. 00-02-17885).

REFERENCES

1. Zh. I. Alferov, Fiz. Tekh. Poluprovodn. (St. Petersburg) **32**, 3 (1998) [Semiconductors **32**, 1 (1998)].
2. S. V. Gaponenko, Fiz. Tekh. Poluprovodn. (St. Petersburg) **30**, 577 (1996) [Semiconductors **30**, 315 (1996)].
3. N. N. Ledentsov, Fiz. Tekh. Poluprovodn. (St. Petersburg) **33**, 1039 (1999) [Semiconductors **33**, 946 (1999)].
4. A. I. Yakimov, V. A. Markov, A. V. Dvurechenskii, and O. P. Pchelyakov, Philos. Mag. B **65**, 701 (1992).
5. N. N. Ledentsov, V. M. Ustinov, V. A. Shchukin, *et al.*, Fiz. Tekh. Poluprovodn. (St. Petersburg) **32**, 385 (1998) [Semiconductors **32**, 343 (1998)].
6. F. Hatami, N. N. Ledentsov, M. Grundmann, *et al.*, Appl. Phys. Lett. **67**, 656 (1995).
7. F. Hatami, M. Grundmann, N. N. Ledentsov, *et al.*, Phys. Rev. B **57**, 4635 (1998).
8. J. M. Rorison, Phys. Rev. B **48**, 4643 (1993).
9. U. E. H. Laheld, F. B. Pedersen, and P. C. Hemmer, Phys. Rev. B **52**, 2697 (1995).
10. S. Fukatsu, H. Sunamura, Y. Shiraki, and S. Komiyama, Appl. Phys. Lett. **71**, 258 (1997).
11. A. V. Kalameœtsev, A. O. Govorov, and V. M. Kovalev, Pis'ma Zh. Éksp. Teor. Fiz. **68**, 634 (1998) [JETP Lett. **68**, 669 (1998)].
12. A. V. Dvurechenskiœ, A. I. Yakimov, V. A. Markov, *et al.*, Izv. Akad. Nauk, Ser. Fiz. **63**, 307 (1999).
13. A. V. Dvurechenskiœ and A. I. Yakimov, Izv. Akad. Nauk, Ser. Fiz. **64**, 306 (2000).
14. O. P. Pchelyakov, Yu. B. Bolkhovityanov, A. V. Dvurechenskiœ, *et al.*, Fiz. Tekh. Poluprovodn. (St. Petersburg) **34**, 1281 (2000) [Semiconductors **34**, 1229 (2000)].
15. A. V. Dvurechenskiœ and A. I. Yakimov, Izv. Vyssh. Uchebn. Zaved., Mater. Élektron. Tekh., No. 4, 4 (1999).
16. A. I. Yakimov, V. A. Markov, A. V. Dvurechenskii, and O. P. Pchelyakov, J. Phys.: Condens. Matter **6**, 2573 (1994).
17. A. V. Rzhanov, *Electron Processes on Semiconductor Surface* (Nauka, Moscow, 1971).
18. D. Bimberg, Fiz. Tekh. Poluprovodn. (St. Petersburg) **33**, 1044 (1999) [Semiconductors **33**, 951 (1999)].
19. M. M. Rieger and P. Vogl, Phys. Rev. B **48**, 14 276 (1993).
20. T. Meyer, M. Klemenc, and H. Von Känel, Phys. Rev. B **60**, R8493 (1999).
21. O. G. Schidt, K. Eberl, and Y. Rau, Phys. Rev. B **62**, 16715 (2000).
22. A. V. Nenashev and A. V. Dvurechenskiœ, Zh. Éksp. Teor. Fiz. **118**, 570 (2000) [JETP **91**, 497 (2000)].
23. P. N. Keating, Phys. Rev. **145**, 637 (1966).
24. Y. Kikuchi, H. Sugii, and K. Shintani, J. Appl. Phys. **89**, 1191 (2001).
25. C. Kittel, *Quantum Theory of Solids* (Wiley, New York, 1963; Nauka, Moscow, 1967).
26. A. I. Yakimov, A. V. Dvurechenskiœ, N. P. Stepina, *et al.*, Zh. Éksp. Teor. Fiz. **119** (3), 574 (2001) [JETP **92**, 500 (2001)].
27. C. G. Van de Walle, Phys. Rev. B **39**, 1871 (1989).
28. A. I. Yakimov, N. P. Stepina, A. V. Dvurechenskii, *et al.*, Semicond. Sci. Technol. **15**, 1125 (2000).
29. R. J. Warbuton, C. S. Dürr, K. Karrai, *et al.*, Phys. Rev. Lett. **79**, 5282 (1997).
30. K. H. Schmidt, G. Medeiros-Ribeiro, and P. M. Petro, Phys. Rev. B **58**, 3597 (1998).
31. M. Grundmann, O. Stier, and D. Bimberg, Phys. Rev. B **52** (16), 11969 (1995).
32. F. V. Gasparyan, Z. N. Adamyan, and V. M. Arutyunyan, *Silicon Photodetectors* (Erevan. Univ., Yerevan, 1989).
33. A. I. Yakimov, A. V. Dvurechenskiœ, A. I. Nikiforov, and O. P. Pchelyakov, Pis'ma Zh. Éksp. Teor. Fiz. **68**, 125 (1998) [JETP Lett. **68**, 135 (1998)].
34. A. I. Yakimov, A. V. Dvurechenskiœ, A. I. Nikiforov, and O. P. Pchelyakov, Pis'ma Zh. Éksp. Teor. Fiz. **72**, 267 (2000) [JETP Lett. **72**, 186 (2000)].
35. A. I. Yakimov, A. V. Dvurechenskii, A. I. Nikiforov, *et al.*, Phys. Rev. B **62**, R16283 (2000).
36. A. F. Ioffe, *Physics of Semiconductors* (Akad. Nauk SSSR, Moscow, 1957; Infosearch, London, 1960).
37. A. M. Danishevskiœ, A. A. Kastal'skiœ, B. S. Ryvkin, *et al.*, Pis'ma Zh. Éksp. Teor. Fiz. **10**, 470 (1969) [JETP Lett. **10**, 302 (1969)].
38. A. F. Gibson and P. N. D. Maggs, J. Phys. D **7**, 292 (1974).
39. S. S. Ishchenko, S. M. Okulov, A. A. Klimov, and Z. D. Kovalyuk, Fiz. Tekh. Poluprovodn. (Leningrad) **17**, 1230 (1983) [Sov. Phys. Semicond. **17**, 776 (1983)].
40. I. Lo, W. C. Mitchel, R. Kaspi, *et al.*, Appl. Phys. Lett. **65**, 1024 (1994).
41. J.-P. Cheng, I. Lo, and W. C. Mitchel, J. Appl. Phys. **76**, 667 (1994).
42. I. Lo, S. J. Chen, Y. C. Lee, *et al.*, Phys. Rev. B **57**, R6819 (1998).
43. S. A. Kaz'min, V. I. Kaœdanov, and S. S. Shevchenko, Fiz. Tekh. Poluprovodn. (Leningrad) **19**, 530 (1985) [Sov. Phys. Semicond. **19**, 328 (1985)].
44. I. I. Zasavitskiœ, B. N. Matsonashvili, and V. T. Trofimov, Fiz. Tekh. Poluprovodn. (Leningrad) **23**, 2019 (1989) [Sov. Phys. Semicond. **23**, 1249 (1989)].
45. A. G. De Oliveira, G. M. Ribeiro, D. A. W. Soares, and H. Chacham, Appl. Phys. Lett. **64**, 2258 (1994).
46. V. G. Kustov, Fiz. Tekh. Poluprovodn. (Leningrad) **10**, 2215 (1976) [Sov. Phys. Semicond. **10**, 1318 (1976)].
47. A. I. Yakimov, A. I. Dvurechenskii, N. P. Stepina, and A. I. Nikiforov, Thin Solid Films **380**, 82 (2000).
48. A. V. Dvurechenskiœ and A. I. Yakimov, Izv. Akad. Nauk, Ser. Fiz. **65**, 187 (2001).
49. A. I. Yakimov, A. V. Dvurechenskii, Yu. Yu. Proskuryakov, *et al.*, Appl. Phys. Lett. **75**, 1413 (1999).
50. P. Boucaud, V. Le. Thanh, S. Sauvage, *et al.*, Appl. Phys. Lett. **74**, 401 (1999).
51. S. Sauvage, P. Boucaud, F. H. Julien, *et al.*, Appl. Phys. Lett. **71**, 2785 (1997).
52. S. Sauvage, P. Boucaud, F. H. Julien, *et al.*, J. Appl. Phys. **84**, 4356 (1998).
53. S. Sauvage, P. Boucaud, J.-M. Gerard, and V. Thierry-Mieg, Phys. Rev. B **58**, 10562 (1998).
54. A. Weber, O. Gauthier-Lafaye, F. H. Julien, *et al.*, Appl. Phys. Lett. **74**, 413 (1999).

55. T. Cho, J.-W. Kim, J.-E. Oh, and S. Hong, in *Technical Digest of the International Electron Devices Meeting, 1998*, p. 441.

56. S. Kim, H. Mohseni, M. Erdtmann, *et al.*, Appl. Phys. Lett. **73**, 963 (1998).

57. A. I. Yakimov, A. I. Dvurechenskii, A. I. Nikiforov, and Yu. Yu. Proskuryakov, J. Appl. Phys. **89** (10), 5676 (2001).

58. R. P. G. Karunasiri, J. S. Park, and K. L. Wang, Appl. Phys. Lett. **59**, 2588 (1991).

59. H. Mohseni, E. Michel, Jan Sandoen, *et al.*, Appl. Phys. Lett. **71**, 1403 (1997).

60. A. I. Yakimov, A. V. Dvurechenskii, A. I. Nikiforov, and O. P. Pchelyakov, Phys. Low-Dimens. Struct. **3/4**, 99 (1999).

61. A. I. Yakimov, C. J. Adkins, R. Boucher, *et al.*, Phys. Rev. B **59**, 12598 (1999).

62. A. I. Yakimov, A. V. Dvurechenskii, A. I. Nikiforov, and C. J. Adkins, Phys. Status Solidi B **218**, 105 (2000).

63. A. I. Yakimov, A. V. Dvurechenskii, V. V. Kirienko, *et al.*, Phys. Rev. B **61**, 10868 (2000).

64. A. V. Dvurechenskiœ, V. A. Zinov'ev, V. A. Kudryavtsev, and Zh. V. Smagina, Pis'ma Zh. Éksp. Teor. Fiz. **72** (3), 190 (2000) [JETP Lett. **72**, 131 (2000)].

Translated by D. Mashovets